
Efficient and Generalized end-to-end Autonomous Driving System with Latent Deep Reinforcement Learning and Demonstrations

Zuojin Tang^{1,2}Xiaoyu Chen³YongQiang Li⁴Jianyu Chen^{1,3*}¹Shanghai Qizhi Institute²College of Computer Science and Technology, Zhejiang University³Institute for Interdisciplinary Information Sciences, Tsinghua University⁴Mogo Auto Intelligence and Telematics Information Technology Co., Ltd

*Corresponding to: jianyuchen@tsinghua.edu.cn

Abstract

An intelligent driving system should dynamically formulate appropriate driving strategies based on the current environment and vehicle status while ensuring system security and reliability. However, methods based on reinforcement learning and imitation learning often suffer from high sample complexity, poor generalization, and low safety. To address these challenges, this paper introduces an **Efficient and Generalized end-to-end Autonomous Driving System (EGADS)** for complex and varied scenarios. The RL agent in our EGADS combines variational inference with normalizing flows, which are independent of distribution assumptions. This combination allows the agent to capture historical information relevant to driving in latent space effectively, thereby significantly reducing sample complexity. Additionally, we enhance safety by formulating robust safety constraints and improve generalization and performance by integrating RL with expert demonstrations. Experimental results demonstrate that, compared to existing methods, EGADS significantly reduces sample complexity, greatly improves safety performance, and exhibits strong generalization capabilities in complex urban scenarios. Particularly, we contributed an expert dataset collected through human expert steering wheel control, specifically using the G29 steering wheel.

1 Introduction

An intelligent autonomous driving systems must be able to handle complex road geometry and topology, complex multi-agent interactions with dense surrounding dynamic objects, and accurately follow the planning and obstacle avoidance. Current, autonomous driving systems in industry are mainly using a highly modularized hand-engineered approach, for example, perception, localization, behavior prediction, decision making and motion control, etc. [43] and [44]. Particularly, the autonomous driving decision making systems are focusing on the non-learning model-based methods, which often requires to manually design a driving policy[17] and [36]. However, the manually designed policy could have two several weaknesses: 1) Accuracy. The driving policy of human heuristics and pre-training model can be suboptimal, which will lead to either conservative or aggressive driving policies. 2) Generality. For different scenarios and complicated tasks, we might need to be redesigned the model policy manually for each new scenario.

To solve those problems, existing works such as Imitation Learning (IL) is most popular approach, which can learn a driving policy by collecting the expert driving data. However, those methods can suffer from the following shortcomings for imitation learning: (1) High training cost and sample complexity. (2) Conservation of driving policy. Due to the collect driving data from the human expert, which can only learn driving skills that are demonstrated in the datasets. (3) Limitation of driving performance. What's more, the driving policy based on Reinforcement Learning (RL) is also popular method in recent years, which can automatically learn and explore without any human expert data in various kinds of different driving cases, and it is possible to have a better performance than imitation learning. However, the existing methods also have some weakness: (1) Existing methods in latent space are based on specific distribution assumptions, whereas distributions in the real world tend to be more flexible, resulting in a failure to learn more precisely about belief values. (2) High costs of learning and exploration. (3) The safety and generalization of intelligent vehicles need further improvement. Combining the advantages of RL and IL, the demonstration of

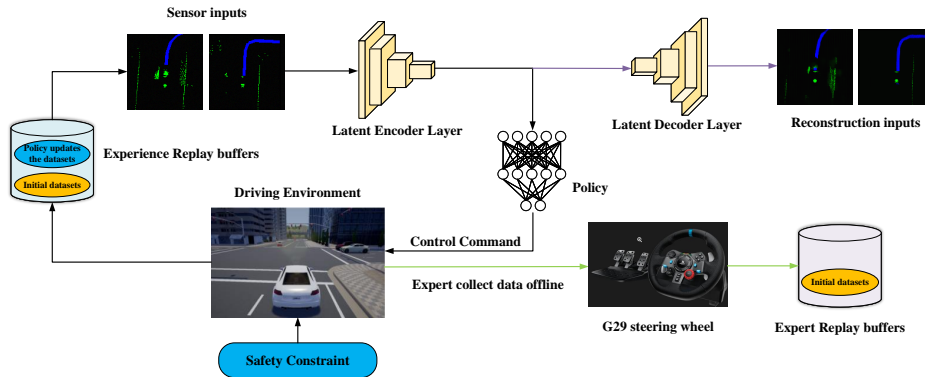


Figure 1: Overview of the efficient and generalized end-to-end autonomous driving with latent reinforcement learning and demonstrations

enhanced RL is not only expected to accelerate Reinforce the initial learning process, but also gain the potential of experts beyond performance. In this paper, we introduce a **Efficient, General end-to-end Autonomous Driving System (EGADS)** for complex and varied scenarios. The RL agent in our SEADS combines variational inference with normalizing flows (NFRL) independent of distribution assumptions, allowing it to sufficiently and flexibly capture historical information useful for driving in latent space, thereby significantly reducing sample complexity. In addition, we have designed the safety constraints of intelligent vehicles. To further increase the upper limit of the overall system, we further enhance the RL search process with a dataset of human experts. In particular, we contributed a dataset of human experts to driving by driving the G29 steering wheel. The experimental results show that compared with the existing methods, our EGADS greatly improves the safety performance, shows strong generalization ability in multiple test maps, and significantly reduces the sample complexity. In summary, our contributions are:

- We present an Efficient, General end-to-end Autonomous Driving System (EGADS) designed for complex and varied scenarios.
- The RL agent in EGADS uses variational inference with normalizing flows (NFRL), independent of distribution assumptions, to capture historical driving information in latent space, significantly reducing sample complexity.
- We designed robust safety constraints for intelligent vehicles to enhance the safety of intelligent vehicle.
- By fine-tuning with a small amount of human expert dataset via using the G29 steering wheel, NFRL agents can learn more general driving principles, significantly improving generalization and reducing sample complexity.

2 Related Work

2.1 Imitation learning

Imitation learning, which utilizes an efficient supervised learning approach, has gained widespread application in autonomous driving research due to its simplicity and effectiveness. For instance, imitation learning has been employed in end-to-end autonomous driving systems that directly generate control signals from raw sensor inputs [11], [32], [5], [12], [3] and [8].

2.2 Reinforcement learning

Deep reinforcement learning (DRL) has demonstrated its strength in addressing complex decision-making and planning problems, leading to a series of breakthroughs in recent years. Researchers have been trying to apply deep RL techniques to the domain of autonomous driving. [29] introduced a continuous control DRL algorithm that trains a deep neural network policy for autonomous driving on a simulated racing track. [46] used Deep Q-Network to learn to steer an autonomous vehicle to keep in the track in simulation. [7] developed a hierarchical DRL framework to handle driving scenarios with intricate decision-making processes, such as navigating traffic lights. [28] marked the first application of DRL in real-world autonomous driving, where they trained a deep lane-keeping policy using only a single front-view camera image as input. [6] proposed an interpretable DRL method for end-to-end autonomous driving. [35] proposed safe navigation. [34] propose a partial end-to-end algorithm that decouples the planning and control tasks. [48] proposes a method to identify and protect unreliable decisions of a DRL driving policy. [47] a framework of constrained multi-agent reinforcement learning with a parallel safety shield for CAVs in challenging driving scenarios. [31] propose the Scene-Rep Transformer to enhance RL decision-making capabilities. The RL frameworks are mostly based on Partially Observable Markov Decision Process (POMDP), such as these [2], [21], [1], [25], [27].

2.3 Reinforcement learning with demonstrations

By combining the advantages of RL and IL is also a relatively popular method in recent years. The techniques outlined in [41] and [45] have proven to be efficient in merging demonstrations and RL for improving learning speed. [30] propose a novel framework combining RL and expert demonstration to learn a motion control strategy for urban scenarios. [23] introduces a predictive behavior planning framework that learns to predict and evaluate from human driving data. [24] propose an enhanced human in-the-loop reinforcement learning method, while they rely on human expert performance and can only accomplish simple scenario tasks. DPAG [37] combines RL and imitation learning to solve complex dexterous manipulation problems. Our approach utilizes the potential for reinforcement learning and normalization flows to learn useful information from historical trajectory information, further learning human expert demonstrations through DPAG methods, and the results provide surprising generalization and performance through a small set of human expert datasets.

3 Methodology

The proposed framework of our EGADS is illustrated in Figure 1. Firstly, human experts collect demonstrations offline using the Logitech G29 steering wheel. These expert demonstrations are then utilized as the RL fine-tuning experience replay buffers for training the entire model. Subsequently, a pre-training process is conducted to establish a model with human expert experience that does not update environmental data during training. The resulting model, enriched with human expert experience, is then used to fine-tune the policy for RL agent. Additionally, we have designed safety constraints for the intelligent vehicle, enhancing its safety performance. Furthermore, we explore 12 different types of images as model inputs, more details can be found in the Appendix A.5.

3.1 Preliminaries

We model the control problem as a Partially Observable Markov Decision Process (POMDP), which is defined using the 7-tuple: $(S, A, T, R, \Omega, O, \gamma)$, where S is a set of states, A is a set of actions, T is a set of conditional transition probabilities between states, R is the reward function, Ω is a set

of observations, O is a set of conditional observation probabilities, and γ is the discount factor. At each timestep $t - 1$, the state of the environment is $s_{t-1} \in S$. The agent takes an action $a_{t-1} \in A$, which causes the environment to transit to state s_t with probability $T(s_t | s_{t-1}, a_{t-1})$. The agent then receives an observation $o_t \in \Omega$ which depends on the new state of the environment s_t with probability $O(o_t | s_t)$. Finally, the agent receives a reward r_{t-1} equal to $R(s_{t-1})$. The goal of the RL agent is to maximize expected cumulative reward $E[\sum_{t=0}^{\infty} \gamma^t r_t]$, γ is the discount factor. After having taken action a_{t-1} and observing o_t , an agent needs to update its belief state, which is defined as the probability distribution of the environment state conditioned on all historical information: $b(s_t) = p(s_t | \tau_t, o_t)$, where $\tau_t = \{o_1, a_1, \dots, o_{t-1}, a_{t-1}\}$.

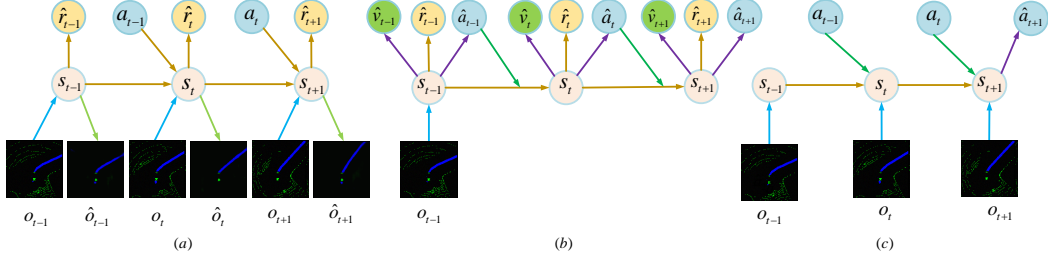


Figure 2: (a) RL Agent learns potential dynamics from past experience datasets. (b) RL Agent predicts driving action in an imaginary space. (c) RL Agent interacts with driving environment.

3.2 Latent dynamic model for autonomous driving

We propose the use of latent variables to solve problems in end-to-end autonomous driving. This potential space is used to encode complex urban driving environments, including visual inputs, spatial features, and road conditions. Historical high-dimensional raw observation data is compressed into this low-dimensional latent space and learned through a sequential latent environment model that learns in conjunction with the maximum entropy RL process. We introduces RL agent model consists of components can be constructed the PGM of POMDP as follow:

$$\begin{aligned}
 \text{State transition model: } & p_{\theta}(s_t | s_{t-1}, a_{t-1}) \\
 \text{Reward model: } & p_{\theta}(r_t | s_t) \\
 \text{Observation model: } & p_{\theta}(o_t | s_t)
 \end{aligned} \tag{1}$$

where p is prior probability, q is posterior probability, o is observations, a is actions, s is latent states and θ is the parameter of the model. Then the world model reconstructs the inputs images from the original sensors, more details can be found in the Appendix A.8.

3.3 RL agent in the latent space

Visual control[42],[39], [4] can be defined as a POMDP. The traditional components of agents that learn through imagination include dynamics learning, behavior learning, and environment interaction[19], [20]. The RL agent in the latent space in our SEADS mainly includes the following:

(1) RL Agent learns potential dynamics from past experience datasets of autonomous vehicle. As shown in Figure 2(a), using p to represent prior probability, q to represent posterior probability, agent learns to encode observations o and actions a into compact latent states s , and \hat{o}_t is reconstructed with $q(\hat{o}_t | s_t)$ while s_t is determined via $p(s_t | s_{t-1}, a_{t-1}, o_t)$.

(2) RL Agent predicts driving action in an imaginary space. As shown in Figure 2(b), RL Agent is in a close latent state space where it can predict value \hat{v}_t , reward \hat{r}_t and action \hat{a}_t based on current input o_{t-1} with $q(\hat{v}_t, \hat{r}_t, \hat{a}_t | s_t)$, $p(s_t | s_{t-1}, \hat{a}_{t-1})$, $q(\hat{a}_{t-1} | s_{t-1})$.

(3) RL Agent interacts with driving environment. As shown in Figure 2(c), RL Agent predicts next action values \hat{a}_{t+1} by encoding historical trajectory information via $q(\hat{a}_{t+1} | s_{t+1})$, $p(s_{t+1} | s_t, a_t, o_{t+1})$.

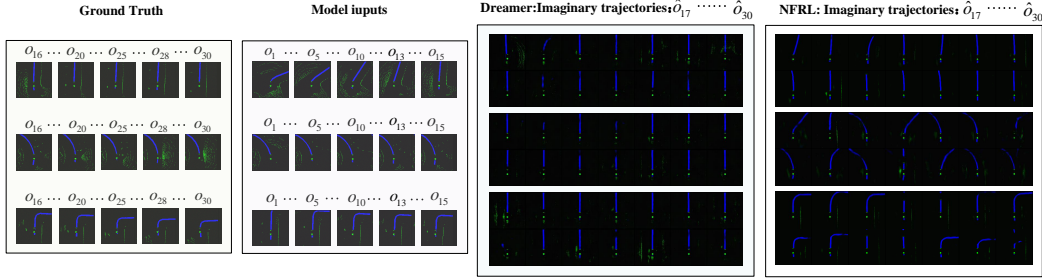


Figure 3: Randomly sample sensor inputs Lidar_noground o_1, o_2, \dots, o_{15} , and then our model can imagine driving behaviors $\hat{o}_{16}, \hat{o}_{17}, \dots, \hat{o}_{30}$. The results show that compared with Dreamer, our NFRL model is more accurate and diverse, with no mode mixup and less blur.

3.4 Normalizing Flow for inferred belief

Existing latent RL models in autonomous driving either suffer from the curse of dimensionality or make some assumptions and only learn approximate distributions. This approximation imposes strong limitations and is problematic, whereas distributions in the real world tend to be more flexible. In the continuous and dynamic space, existing methods based on Normalizing Flows(NF)[14], [22], [38] can learn more flexible and generalized beliefs. These methods provide a solid foundation for RL agents to accurately predict future driving actions. Inspired by [10], we added a belief inference model: $q_\theta(s_t|\tau_t, o_t)$, where θ is the parameter of the model. The belief model can be substituted the probability density with normalizing flow in the KL-divergence term of Equation 2.

$$q_K(s_t|\tau_t, o_t) = \log q_0(s_t|\tau_t, o_t) - \sum_{k=1}^K \left| \det \frac{\partial f_{\psi_k}}{\partial s_{t,k-1}} \right| \quad (2)$$

$$p_K(s_t|\tau_t) = \log p_0(s_t|\tau_t) - \sum_{k=1}^K \left| \det \frac{\partial f_{\omega_k}}{\partial s_{t,k-1}} \right|$$

Where $q_0 = q_\theta$, $q_K = q_{\theta, \psi}$, $p_0 = p_\theta$, $p_K = p_{\theta, \omega}$, ψ and ω are the parameters of a series of mapping transformations of the posterior and prior distributions. Where $\tau_t = \{o_1, a_1, \dots, o_{t-1}, a_{t-1}\}$. The input images $o_{1:t}$ and actions $a_{1:t-1}$ are encoded with $q_\theta(s_t|\tau_t, o_t)$. Then the final inferred belief is obtained by propagating $q_\theta(s_t|\tau_t, o_t)$ through a set of NF mappings denoted $f_{\psi_K} \dots f_{\psi_1}$ to get a posterior distribution $q_{\theta, \psi}(s_t|\tau_t, o_t)$. The final prior is obtained by propagating $p_\theta(s_t|\tau_t)$ through a set of NF mappings denoted $f_{\omega_K} \dots f_{\omega_1}$ to get a prior distribution $p_{\theta, \omega}(s_t|\tau_t)$. Where $p_K(s_t|\tau_t) = p_K(s_t|s_{t-1}, a_{t-1})$, given the sampled s_{t-1} from $q_K(s_{1:t}|\tau_t, o_t)$. Finally, our normalizing flow inference RL model(NFRL) is optimized by variational inference method, in which the evidence lower bound (ELBO)[26],[13] is maximized. The loss function is defined as:

$$\mathcal{M}_{\text{model}}(\theta, \psi, \omega) = \sum_{t=1}^T (\mathbb{E}_{q(s_t|o_{\leq t}, a_{< t})} [\log p_\theta(o_t | s_t) + \log p_\theta(r_t | s_t)] - \mathbb{E}_{q_K(s_{1:T}|o_{1:T}, a_{1:T-1})} [D_{\text{KL}}(q_K(s_t | \tau_t, o_t) || p_K(s_t | \tau_t, o_t))]) \quad (3)$$

3.5 Policy optimization

The action model implements the policy and is designed to predict the actions that are likely to be effective in responding to the simulated environment. The value model estimates the expected reward generated by the behavior model at each state s_τ .

$$a_\tau \sim q_\phi(a_\tau | s_\tau), \quad v_\eta(s_\tau) = E_{q_\phi} \left[\sum_{t=\tau}^{t+H} \gamma^{\tau-t} r_\tau \right] \quad (4)$$

Where ϕ, η are the parameters of the approximated policy and value. The objective of the action model is to use high value estimates to predict action that result in state trajectories

$$\mathcal{M}_{\text{actor}}(\phi) = E_{q_\phi} \left(\sum_{\tau=t}^{t+H} V_\tau^\lambda \right) \quad (5)$$

To update the action and value models, we calculate the value estimate $v_\eta(s_\tau)$ for all states s_τ along the imagined trajectory. V_τ^λ can be defined as follow:

$$V_\tau^\lambda = (1 - \tau)v_\eta(s_{\tau+1}) + \lambda V_{\tau+1}^\lambda, \quad \tau < t + H \quad (6)$$

Then we can train the critic to regress the TD(λ) [40] target return via a mean squared error loss:

$$\mathcal{M}_{\text{critic}}(\eta) = \mathbb{E} \left[\sum_{\tau=t}^{t+H} \frac{1}{2} \left(v_\eta(s_\tau) - V_\tau^\lambda \right)^2 \right] \quad (7)$$

Where η denote the parameters of the critic network and H is the prediction horizon. Then the loss function is as follows:

$$\min_{\psi, \eta, \phi, \theta, \omega, \eta} \alpha_0 \mathcal{M}_{\text{critic}}(\eta) - \alpha_1 \mathcal{M}_{\text{actor}}(\phi) - \alpha_2 \mathcal{M}_{\text{model}}(\theta, \psi, \omega) \quad (8)$$

We jointly optimize the parameters of model loss ψ, θ, ω , critic loss η and actor loss ϕ , where $\alpha_0, \alpha_1, \alpha_2$ are coefficients for different components.

In order to accurately evaluate our model prediction of driving actions for intelligent vehicle, this problem can be viewed as a special POMDP problem with the reward value maintained at 0. As shown in Figure 3, the result shows that our model can accurately predict future driving actions.

3.6 Safety constraint

In the Gym-Carla benchmark, the reward function proposed by [9] is denoted as f_1 . To ensure the intelligent vehicle operates safely and smoothly in complex environments, we incorporated additional safety and robustness constraints into f_1 , denoted as f_2 . These constraints include time to collision and smooth steering. For detailed information on f_1 and f_2 , please refer to Appendix A.6.

(1)Front time to collision. When around vehicles are within the distance of ego vehicle (our agent vehicle) head in our setting, then we can calculate the front time to collision between ego vehicle and around vehicles. Firstly, the speed and steering vector $(s_\tau, a_\tau) \in \mathbb{S}$ of the ego vehicle are defined, where s_τ represents the angle vector of vehicle steering and a_τ represents the acceleration vector of the vehicle in local coordinate system. Secondly, two waypoints closest to the current ego vehicle are selected from the given navigation routing as direction vectors \vec{w}_p for the entire route progression, where \rightarrow indicates a vector in world coordinates. The position vectors for both ego vehicle and around vehicles are represented by $(\vec{x}_t^*, \vec{y}_t^*)$, respectively. Finally, δ_e and δ_a representing angles between position vectors for ego vehicle and around vehicles with respect to \vec{w}_p are calculated respectively.

$$\begin{aligned} \vec{w}_p &= \left[\left(\frac{w_{t+1}^x - w_t^x}{2} \right) - (w_t^x), \left(\frac{w_{t+1}^y - w_t^y}{2} \right) - (w_t^y) \right] \\ \delta_e &= \frac{[v_t^{\vec{x}*}, v_t^{\vec{y}*}] \cdot \vec{w}_p}{\|v_t^{\vec{x}*}, v_t^{\vec{y}*}\|_2 \|\vec{w}_p\|_2}, \delta_a = \frac{[v_t^{\vec{x}}, v_t^{\vec{y}}] \cdot \vec{w}_p}{\|v_t^{\vec{x}}, v_t^{\vec{y}}\|_2 \|\vec{w}_p\|_2} \end{aligned} \quad (9)$$

Where, l is the length of the set of waypoints \mathbb{W} stored. The variable $t \in \tau$, and $w_t^x \in \mathbb{W}_1$ represents the x coordinate of the first navigation point closest to the intelligent vehicle on its current route at time t . Similarly, $w_{t+1}^x \in \mathbb{W}_2$. Furthermore, it is possible to calculate the F_{ttc} as follows:

$$F_{ttc} = \frac{\|\vec{x}_t - \vec{x}_t^*, \vec{y}_t - \vec{y}_t^*\|_2}{\left| \|v_t^{\vec{x}*}, v_t^{\vec{y}*}\|_2 \sin(\delta_e) - \|v_t^{\vec{x}}, v_t^{\vec{y}}\|_2 \sin(\delta_a) \right|} \quad (10)$$

(2)Lateral time to collision. When around vehicles are not within the distance of ego vehicle head in our setting, we consider significantly the L_{ttc} . The calculation method for L_{ttc} and F_{ttc} is the same. However, the collision constraint effect of L_{ttc} on intelligent vehicle is limited, mainly due to the slow reaction time of intelligent vehicle to L_{ttc} , lack of robustness and generalization ability. Therefore, we have implemented a method of assigning values to different intervals for L_{ttc} as follows:

$$\begin{cases} \min(z_\tau, c_\tau + 1.0), & \nu_g \leq (c_\tau - 1.5) \text{ and } \mu_a \leq (c_\tau - 0.5). \\ \min(z_\tau, c_\tau - 1.8), & \nu_g \leq (c_\tau - 3.0) \text{ and } \mu_a \leq (c_\tau - 2.0). \\ \min(z_\tau, c_\tau - 3.0), & \nu_g \leq (c_\tau - 3.5) \text{ and } \mu_a \leq (c_\tau - 3.0). \end{cases} \quad (11)$$

Where c_τ is the empirical const of L_{ttc} in our setting at (5,7), z_τ is the ttc based on their combined speed. ν_g is the ttc obtained by calculating the longitudinal velocity. μ_a is the ttc obtained by calculating the lateral velocity.

(3) Smooth steering is defined as $|s_t^\delta - s_t^{*\delta}| \in e_c$. s_t^δ is the actual steering angle. $s_t^{*\delta}$ is the predicted steering angle based on policy π . The range of e_c can be established based on empirical data.

3.7 Augmenting RL policy with demonstrations

Though, NFRL can significantly reduce complexity, and reward design based on security constraints can enhance safety. Demonstrations can mitigate the need for painstaking reward shaping, guide exploration, further reduce sample complexity, and help generate robust, natural behaviors. We propose the demonstration augmented RL agent method which incorporates demonstrations into RL agent in two ways:

(1) Pretraining with behavior cloning. we use behavior cloning to provide a policy π^* via expert demonstrations and then to train a model $\mathcal{M}_{\text{expert}}$ with some expert ability.

$$\mathcal{M}_{\text{expert}} = \underset{\xi}{\text{maximize}} \sum_{(s', a') \in \pi^*(\mathcal{D}_e)} \ln \pi_\xi^*(a'_\tau | s'_\tau) \quad (12)$$

where \mathcal{D}_e is a human expert dataset obtained from driving G29 steering.

(2) RL fine-tuning with augmented loss: we employ $\mathcal{M}_{\text{expert}}$ to initialize a model trained by deep RL policies, which reduces the sampling complexity of the deep RL policy. The training loss of the actor model as follows:

$$\mathcal{M}_{\text{actor}}(\phi, \xi) = \mathcal{M}_{\text{actor}}(\phi) + k \ln \pi_\xi^*(a'_\tau | s'_\tau), (a'_\tau, s'_\tau) \in \mathcal{D}_e \quad (13)$$

Where k represents the balance between the cloning policy and latent deep RL policy, and is set as a constant based on empirical data. We only changed the actor model of NFRL, and the optimization of the other parts is exactly the same.

4 Experiment

In this section, first, the environment setup is introduced. Second, we describe the essential details of implementation. Finally, the evaluation results are presented and discussed.

4.1 Experiment setup

The model training in this paper is deployed on systems including Python=3.6, Pytorch-gpu=1.5.0, GeForce RTX-3090 running on Linux. In order to evaluate the performance of our EGADS in addressing challenges related to sampling efficiency, safety, we respectively designed corresponding experiments to answer each of these questions. Our experiments were conducted on a benchmark called "Gym-carla," a third-party environment for OpenAI gym that is used with the CARLA simulator[15]. Additionally, unlike the official CARLA leaderboard, gym-carla can conveniently verify RL algorithms. In order to comprehensively evaluate the performance of our EGADS, we utilized five maps in CARLA, including town01, town03, town04, town05 and town06, as illustrated for details in Appendix A.3. We present the hyperparameter settings for the methods in Appendix A.7. Particularly, we contributed an expert dataset \mathcal{D}_e collected through human expert steering wheel control, with further details provided in Appendix A.4.

4.2 Measure Driving Performance Metrics

To evaluate our autonomous driving system more realistically, we adopted an approach that involves randomly generating driving routes, resetting the coordinates of all vehicles on the map, and randomizing the driving scenarios in each episode. In the Gym-Carla benchmark, an episode terminates under any of the following conditions: the number of collisions exceeds one, the maximum number of time steps is reached, the destination is reached, the cumulative lateral deviation from the lane exceeds 10 meters, or the vehicle remains stationary for 50 seconds. Given that this benchmark does not set a specific destination and the driving routes are randomly assigned, we use the Safe Driving Distance as a performance metric. This metric represents the cumulative distance that the intelligent vehicle can travel safely in each episode without triggering a termination condition. We calculate

Table 1: In the training stage, the steps and times for all methods are compared under different baseline Average Safe Driving Distance(ASD) in Town03(max episodes length=500). Particularly, $+\infty$ means the situation where the training time has exceeded 250hours and the model has still not reached the baseline.

Method	Reward shaping	ASD=50m		ASD=100m		ASD=150m		ASD=200m	
		episodes↓	times↓	episodes↓	times↓	episodes↓	times↓	episodes↓	times↓
DDPG	f_1	$+\infty$	$+\infty$	$+\infty$	$+\infty$	$+\infty$	$+\infty$	$+\infty$	$+\infty$
SAC	f_1	$+\infty$	$+\infty$	$+\infty$	$+\infty$	$+\infty$	$+\infty$	$+\infty$	$+\infty$
TD3	f_1	≥ 161	$\geq 192\text{h}$	$+\infty$	$+\infty$	$+\infty$	$+\infty$	$+\infty$	$+\infty$
DQN	f_1	≥ 163	$\geq 53\text{h}$	$+\infty$	$+\infty$	$+\infty$	$+\infty$	$+\infty$	$+\infty$
Latent_SAC	f_1	≥ 167	$\geq 43\text{h}$	≥ 352	$\geq 105\text{h}$	≥ 1005	$\geq 212\text{h}$	$+\infty$	$+\infty$
Dreamer	f_1	$+\infty$	$+\infty$	$+\infty$	$+\infty$	$+\infty$	$+\infty$	$+\infty$	$+\infty$
NFRL(our base)	f_1	≥ 141	$\geq 21\text{h}$	≥ 121	$\geq 65\text{h}$	$+\infty$	$+\infty$	$+\infty$	$+\infty$
NFRL+SC	f_2	≥ 71	$\geq 12\text{h}$	≥ 301	$\geq 40\text{h}$	≥ 761	$\geq 78\text{h}$	≥ 1100	$\geq 146\text{h}$
BC+Demo	<i>no</i>	$+\infty$	$+\infty$	$+\infty$	$+\infty$	$+\infty$	$+\infty$	$+\infty$	$+\infty$
NFRL+SC+Demo	f_2	≥ 21	$\geq 1.3\text{h}$	≥ 58	$\geq 3\text{h}$	≥ 139	$\geq 9\text{h}$	≥ 321	$\geq 48\text{h}$

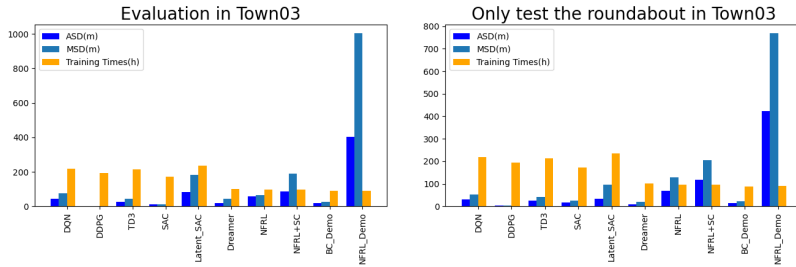


Figure 4: We compared performance in random scenarios in Town03 and scenarios limited to roundabouts

the Average Safe Driving Distance (ASD) and Maximum Safe Driving Distance (MSD) over M episodes. ASD and MSD, being independent of the specific form of the reward function, provide a more accurate reflection of performance across different methods.

$$ASD = \frac{1}{M} \left(\sum_{i=1}^M \sum_{t=0}^N v_t * d_t \right), MSD = \max \left(\sum_{i=1}^M \sum_{t=0}^N v_t * d_t \right) \quad (14)$$

where N represents the maximum sequence length of an episode, v_t denotes the velocity of the vehicle, and d_t denotes the time interval between two consecutive frames, with a value of 0.1 seconds.

4.3 Comparison settings

In order to evaluate the performance of our autonomous driving system more effectively, we have conducted various comparisons with existing methods such as DDPG[29], SAC[18], TD3[16], DQN[33], Latent_SAC[6], Dreamer[19]. We decomposed EGADS into four components, variational inference based on normalizing flows RL agent(NFRL), safety constraints (SC), behavior cloning (BC), augmenting RL policy with demonstrations. We then conducted evaluations using four comparison settings, NFRL, NFRL+SC, BC+Demo, NFRL+SC+Demo. BC+Demo indicates the use of behavioral cloning to imitate the expert dataset, while NFRL+SC+Demo involves using expert datasets to augment the NFRL policy combined with safety constraints.

4.4 Experimental result and discussion

During the training phase, as shown in Table 1, our NFRL method demonstrated at least 2 times increase in training time efficiency when reaching the 50m and 100m baselines compared to other RL methods. However, it did not reach the 150m baseline due to frequent collision problems observed during the experiments. To address this, we designed a reward function with safety constraints (SC). In experiments, NFRL+SC achieved all four baselines with efficiency improvements over NFRL.

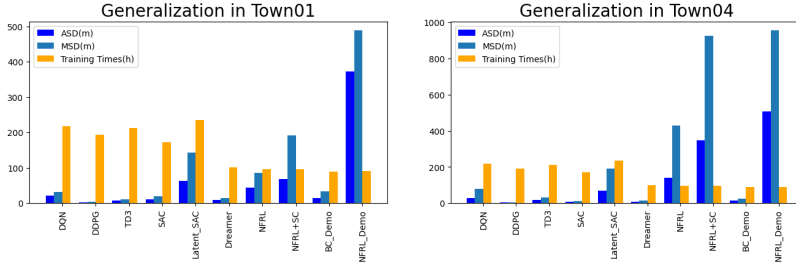


Figure 5: We initially train all methods in Town03 and evaluate respectively in Town01 and Town04

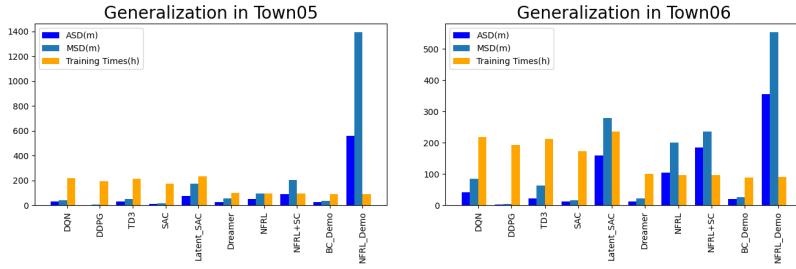


Figure 6: We initially train all methods in Town03 and evaluate respectively in Town05 and Town06

Additionally, only NFRL+SC reached the 200m baseline, demonstrating that SC not only enhances safety but also reduces sample complexity.

Behavior cloning(BC) does not guarantee the effectiveness of the cloned policy due to distribution shifts between the demonstration and the agent policy. Our experiments showed that BC generally failed, as evidenced by methods like BC+Demo not reaching any of the four baselines. However, NFRL+SC+Demo significantly reduced sample complexity and outperformed other methods across all four baselines.

As shown in Figure 4, during the testing phase, we compared performance in random scenarios in Town03 and scenarios limited to roundabouts. Our NFRL series methods consistently reduced sample complexity and enhanced safety compared to existing methods. To evaluate generalization, all methods were trained in Town03 and then evaluated in Town01, Town04, Town05, and Town06, as illustrated in Figures 5 and 6. Results showed that our NFRL series demonstrated excellent generalization capabilities. Particularly, NFRL+SC+Demo exhibited outstanding performance in safety, efficiency, and generalization, significantly outperforming NFRL+SC and BC+Demo. This suggests that while behavioral cloning provides a good initialization for NFRL, it does not fully leverage the information in demonstration data. For instance, expert demonstration data, although collected in different driving environments, can offer general driving strategies such as slowing down when an obstacle is ahead, decelerating before turns, and accelerating uphill. BC cannot learn these general behaviors from limited data, and important information is lost when used only for initialization. Once NFRL understands the environment, demonstration data should guide it in learning these general driving principles.

Although NFRL+SC+Demo demonstrates strong overall performance compared to other RL methods, including NFRL+SC and BC+Demo, this comparison may not be entirely fair. Nonetheless, our approach offers valuable insights for autonomous driving system design. By fine-tuning with a small amount of high-quality data, NFRL agents can learn more general driving principles, significantly improving generalization and reducing sample complexity. Additionally, incorporating a safety controller can enhance system safety. Finally, we discuss the broader impacts and limitations of this paper in Appendix A.1 and Appendix A.2.

5 Conclusion

In summary, our EGADS framework addresses the challenges of low sample efficiency, low safety, and limited generalization in autonomous driving. The inclusion of safety constraints significantly enhances vehicle safety. NFRL, our proposed method, accurately predicts future driving actions, reducing sample complexity. By fine-tuning with a small amount of expert data, NFRL agents learn more general driving principles, which greatly improve generalization and sample complexity reduction, offering valuable insights for autonomous driving system design.

References

- [1] Ali-Akbar Agha-Mohammadi, Suman Chakravorty, and Nancy M Amato. Firm: Sampling-based feedback motion-planning under motion uncertainty and imperfect measurements. *The International Journal of Robotics Research*, 33(2):268–304, 2014.
- [2] Karl Johan Åström. Optimal control of markov processes with incomplete state information. *Journal of mathematical analysis and applications*, 10(1):174–205, 1965.
- [3] Mayank Bansal, Alex Krizhevsky, and Abhijit Ogale. Chauffeurnet: Learning to drive by imitating the best and synthesizing the worst. *arXiv preprint arXiv:1812.03079*, 2018.
- [4] Thomas Bengtsson, Peter Bickel, and Bo Li. Curse-of-dimensionality revisited: Collapse of the particle filter in very large scale systems. In *Probability and statistics: Essays in honor of David A. Freedman*, volume 2, pages 316–335. Institute of Mathematical Statistics, 2008.
- [5] Mariusz Bojarski, Davide Del Testa, Daniel Dworakowski, Bernhard Firner, Beat Flepp, Praseon Goyal, Lawrence D Jackel, Mathew Monfort, Urs Muller, Jiakai Zhang, et al. End to end learning for self-driving cars. *arXiv preprint arXiv:1604.07316*, 2016.
- [6] Jianyu Chen, Shengbo Eben Li, and Masayoshi Tomizuka. Interpretable end-to-end urban autonomous driving with latent deep reinforcement learning. *IEEE Transactions on Intelligent Transportation Systems*, 23(6):5068–5078, 2021.
- [7] Jianyu Chen, Zining Wang, and Masayoshi Tomizuka. Deep hierarchical reinforcement learning for autonomous driving with distinct behaviors. In *2018 IEEE Intelligent Vehicles Symposium*, pages 1239–1244. IEEE, 2018.
- [8] Jianyu Chen, Bodi Yuan, and Masayoshi Tomizuka. Deep imitation learning for autonomous driving in generic urban scenarios with enhanced safety. In *2019 IEEE/RSJ International Conference on Intelligent Robots and Systems*, pages 2884–2890. IEEE, 2019.
- [9] Jianyu Chen, Bodi Yuan, and Masayoshi Tomizuka. Model-free deep reinforcement learning for urban autonomous driving. In *2019 IEEE Intelligent Transportation Systems Conference*, pages 2765–2771. IEEE, 2019.
- [10] Xiaoyu Chen, Yao Mark Mu, Ping Luo, Shengbo Li, and Jianyu Chen. Flow-based recurrent belief state learning for pomdps. In *International Conference on Machine Learning*, pages 3444–3468. PMLR, 2022.
- [11] Felipe Codevilla, Matthias Müller, Alexey Dosovitskiy, Antonio M. López, and Vladlen Koltun. End-to-end driving via conditional imitation learning. *2018 IEEE International Conference on Robotics and Automation (ICRA)*, pages 1–9, 2017.
- [12] Felipe Codevilla, Matthias Müller, Antonio López, Vladlen Koltun, and Alexey Dosovitskiy. End-to-end driving via conditional imitation learning. In *2018 IEEE International Conference on Robotics and Automation*, pages 4693–4700. IEEE, 2018.
- [13] Nicola De Cao, Wilker Aziz, and Ivan Titov. Block neural autoregressive flow. In *Uncertainty in artificial intelligence*, pages 1263–1273. PMLR, 2020.
- [14] Laurent Dinh, Jascha Sohl-Dickstein, and Samy Bengio. Density estimation using real nvp. *arXiv preprint arXiv:1605.08803*, 2016.

- [15] Alexey Dosovitskiy, German Ros, Felipe Codevilla, Antonio Lopez, and Vladlen Koltun. Carla: An open urban driving simulator. In *Conference on Robot Learning*, pages 1–16. PMLR, 2017.
- [16] Scott Fujimoto, Herke Hoof, and David Meger. Addressing function approximation error in actor-critic methods. In *International conference on machine learning*, pages 1587–1596. PMLR, 2018.
- [17] David González, Joshué Pérez, Vicente Milanés, and Fawzi Nashashibi. A review of motion planning techniques for automated vehicles. *IEEE Transactions on Intelligent Transportation Systems*, 17(4):1135–1145, 2015.
- [18] Tuomas Haarnoja, Aurick Zhou, Pieter Abbeel, and Sergey Levine. Soft actor-critic: Off-policy maximum entropy deep reinforcement learning with a stochastic actor. In *International conference on machine learning*, pages 1861–1870. PMLR, 2018.
- [19] Danijar Hafner, Timothy Lillicrap, Jimmy Ba, and Mohammad Norouzi. Dream to control: Learning behaviors by latent imagination. *arXiv preprint arXiv:1912.01603*, 2019.
- [20] Danijar Hafner, Timothy Lillicrap, Ian Fischer, Ruben Villegas, David Ha, Honglak Lee, and James Davidson. Learning latent dynamics for planning from pixels. In *International conference on machine learning*, pages 2555–2565. PMLR, 2019.
- [21] Geoffrey A Hollinger and Gaurav S Sukhatme. Sampling-based robotic information gathering algorithms. *The International Journal of Robotics Research*, 33(9):1271–1287, 2014.
- [22] Chin-Wei Huang, David Krueger, Alexandre Lacoste, and Aaron Courville. Neural autoregressive flows. In *International Conference on Machine Learning*, pages 2078–2087. PMLR, 2018.
- [23] Zhiyu Huang, Haochen Liu, Jingda Wu, and Chen Lv. Conditional predictive behavior planning with inverse reinforcement learning for human-like autonomous driving. *IEEE Transactions on Intelligent Transportation Systems*, 2023.
- [24] Zilin Huang, Zihao Sheng, Chengyuan Ma, and Sikai Chen. Human as ai mentor: Enhanced human-in-the-loop reinforcement learning for safe and efficient autonomous driving. *arXiv preprint arXiv:2401.03160*, 2024.
- [25] Vadim Indelman, Luca Carlone, and Frank Dellaert. Planning in the continuous domain: A generalized belief space approach for autonomous navigation in unknown environments. *The International Journal of Robotics Research*, 34(7):849–882, 2015.
- [26] Michael I Jordan, Zoubin Ghahramani, Tommi S Jaakkola, and Lawrence K Saul. An introduction to variational methods for graphical models. *Learning in graphical models*, pages 105–161, 1998.
- [27] Maximilian Karl, Maximilian Soelch, Justin Bayer, and Patrick Van der Smagt. Deep variational bayes filters: Unsupervised learning of state space models from raw data. *arXiv preprint arXiv:1605.06432*, 2016.
- [28] Alex Kendall, Jeffrey Hawke, David Janz, Przemyslaw Mazur, Daniele Reda, John-Mark Allen, Vinh-Dieu Lam, Alex Bewley, and Amar Shah. Learning to drive in a day. In *2019 International Conference on Robotics and Automation*, pages 8248–8254. IEEE, 2019.
- [29] Timothy P Lillicrap, Jonathan J Hunt, Alexander Pritzel, Nicolas Heess, Tom Erez, Yuval Tassa, David Silver, and Daan Wierstra. Continuous control with deep reinforcement learning. *arXiv preprint arXiv:1509.02971*, 2015.
- [30] Haochen Liu, Zhiyu Huang, and Chen Lv. Improved deep reinforcement learning with expert demonstrations for urban autonomous driving. *2022 IEEE Intelligent Vehicles Symposium (IV)*, pages 921–928, 2021.
- [31] Haochen Liu, Zhiyu Huang, Xiaoyu Mo, and Chen Lv. Augmenting reinforcement learning with transformer-based scene representation learning for decision-making of autonomous driving. *arXiv preprint arXiv:2208.12263*, 2022.

- [32] Luc Le Mero, Dewei Yi, Mehrdad Dianati, and Alexandros Mouzakitis. A survey on imitation learning techniques for end-to-end autonomous vehicles. *IEEE Transactions on Intelligent Transportation Systems*, 23:14128–14147, 2022.
- [33] Volodymyr Mnih, Koray Kavukcuoglu, David Silver, Andrei A Rusu, Joel Veness, Marc G Bellemare, Alex Graves, Martin Riedmiller, Andreas K Fidjeland, Georg Ostrovski, et al. Human-level control through deep reinforcement learning. *nature*, 518(7540):529–533, 2015.
- [34] Andrew Murdoch, Johannes Cornelius Schoeman, and Hendrik Willem Jordaan. Partial end-to-end reinforcement learning for robustness against modelling error in autonomous racing. *arXiv preprint arXiv:2312.06406*, 2023.
- [35] Ghadi Nehme and Tejas Y Deo. Safe navigation: Training autonomous vehicles using deep reinforcement learning in carla. *arXiv preprint arXiv:2311.10735*, 2023.
- [36] Brian Paden, Michal Čáp, Sze Zheng Yong, Dmitry Yershov, and Emilio Frazzoli. A survey of motion planning and control techniques for self-driving urban vehicles. *IEEE Transactions on Intelligent Vehicles*, 1(1):33–55, 2016.
- [37] Aravind Rajeswaran, Vikash Kumar, Abhishek Gupta, Giulia Vezzani, John Schulman, Emanuel Todorov, and Sergey Levine. Learning complex dexterous manipulation with deep reinforcement learning and demonstrations. *arXiv preprint arXiv:1709.10087*, 2017.
- [38] Danilo Rezende and Shakir Mohamed. Variational inference with normalizing flows. In *International conference on machine learning*, pages 1530–1538. PMLR, 2015.
- [39] David Silver and Joel Veness. Monte-carlo planning in large pomdps. *Advances in neural information processing systems*, 23, 2010.
- [40] Richard S Sutton and Andrew G Barto. *Reinforcement learning: An introduction*. MIT press, 2018.
- [41] Evangelos Theodorou, Jonas Buchli, and Stefan Schaal. Reinforcement learning of motor skills in high dimensions: A path integral approach. In *2010 IEEE International Conference on Robotics and Automation*, pages 2397–2403. IEEE, 2010.
- [42] Sebastian Thrun. Monte carlo pomdps. *Advances in neural information processing systems*, 12, 1999.
- [43] Sebastian Thrun, Mike Montemerlo, Hendrik Dahlkamp, David Stavens, Andrei Aron, James Diebel, Philip Fong, John Gale, Morgan Halpenny, Gabriel Hoffmann, et al. Stanley: The robot that won the darpa grand challenge. *Journal of field Robotics*, 23(9):661–692, 2006.
- [44] Chris Urmson, Joshua Anhalt, Drew Bagnell, Christopher Baker, Robert Bittner, MN Clark, John Dolan, Dave Duggins, Tugrul Galatali, Chris Geyer, et al. Autonomous driving in urban environments: Boss and the urban challenge. *Journal of field Robotics*, 25(8):425–466, 2008.
- [45] Herke Van Hoof, Tucker Hermans, Gerhard Neumann, and Jan Peters. Learning robot in-hand manipulation with tactile features. In *2015 IEEE-RAS 15th International Conference on Humanoid Robots (Humanoids)*, pages 121–127. IEEE, 2015.
- [46] Peter Wolf, Christian Hubschneider, Michael Weber, André Bauer, Jonathan Härtl, Fabian Dürr, and J Marius Zöllner. Learning how to drive in a real world simulation with deep q-networks. In *2017 IEEE Intelligent Vehicles Symposium*, pages 244–250. IEEE, 2017.
- [47] Zhili Zhang, Songyang Han, Jiangwei Wang, and Fei Miao. Spatial-temporal-aware safe multi-agent reinforcement learning of connected autonomous vehicles in challenging scenarios. In *2023 IEEE International Conference on Robotics and Automation*, pages 5574–5580. IEEE, 2023.
- [48] Weitao Zhou, Zhong Cao, Nanshan Deng, Kun Jiang, and Diange Yang. Identify, estimate and bound the uncertainty of reinforcement learning for autonomous driving. *IEEE Transactions on Intelligent Transportation Systems*, 2023.

A Appendix

In the appendix, we provide more details regarding the efficient and generalized end-to-end autonomous driving system with latent deep reinforcement Learning and demonstrations in the paper, including

- In Subsection A.1 and A.2, we discuss the broader impacts and limitations of this paper.
- In Subsection A.3, we provide a detailed description of the maps used for training in Gym-Carla.
- In Subsection A.4, we explain how we collected the expert demonstration dataset in CARLA using a human expert driving with the G29 steering wheel.
- In Subsection A.5, we explore the impact of up to 12 different data input types on the performance of the NFRL agent.
- In Subsection A.6, we introduce our reward function with safety constraints.
- In Subsection A.7, we present the hyperparameter settings for the methods involved in our experiments.
- In Subsection A.8, we demonstrate the reconstruction of original sensor input images by our NFRL.
- In Subsection A.9, we provide additional results on predictions of future driving actions for NFRL in the imagination space.

A.1 Broader impacts

This paper focuses on the application and research of latent reinforcement learning in end-to-end autonomous driving systems. The goal of this work is to provide meaningful insights and designs to address the high sample complexity, low safety, and poor generalization challenges faced by current end-to-end autonomous driving systems. Overall, this work does not have any negative societal impacts.

A.2 Limitations

This paper presents the design of an efficient and generalized end-to-end autonomous driving system. The safety control still relies on manually designed constraints, and the current reinforcement learning agent is highly sensitive to the coefficients of the reward function, lacking robustness. For low-level control, it might need to be combined with traditional control algorithms to perform effectively. Additionally, all our tests were conducted in a simulated environment and not in real-world scenarios, thus it cannot be directly applied to real autonomous vehicles. Moreover, in our tests, we only considered moving obstacles as vehicles, without considering pedestrians or incorporating traffic rules, indicating that our system still has room for improvement. Nonetheless, we believe that our design, which leverages a small amount of high-quality data to enhance RL, demonstrates strong generalization capabilities. The combination of NFRL and SC can efficiently complete driving tasks in complex environments, providing valuable insights for the design of end-to-end autonomous driving systems.

A.3 Training CARLA maps

In order to comprehensively evaluate the performance of our EGADS, we utilized five maps in CARLA, including Town01, Town03, Town04, Town05 and Town06 as shown in Figure 7. Town01, a small, simple town with a river and several bridges. Town02, a small simple town with a mixture of residential and commercial buildings. Town04, a small town embedded in the mountains with a special infinite highway. Town05, squared-grid town with cross junctions and a bridge. Town06, long many lane highways with many highway entrances and exits. Particularly, Town03 is the most complex town with a 5-lane junction, a roundabout, unevenness, a tunnel, and more.



Figure 7: The road networks of the CARLA include routes for Town01, Town02, Town03, Town04, Town05, and Town06, as well as more complex scenarios in Town03, Town04, and Town05

A.4 Collect expert datasets

CARLA can be operated and controlled through using the python API. Figure 8 shows that we establish a connection between the Logitech G29 steering wheel and the CARLA, and then human expert can collect the datasets of teaching via the G29 steering wheel. Specifically, we linearly map accelerator pedals, brake pedals, and turning angles into $accel[0,3](min,max)$, $brake[-8,0](min,max)$, $steer[-1,1](left,right)$. The tensors are written into user-built Python scripts and combined with CARLA built-in Python API so that users can provide input from their steering wheels to autonomous driving cars in CARLA simulator for \mathcal{D}_{expert} collection. Particularly, we contributed a dataset collected through human expert steering wheel control.

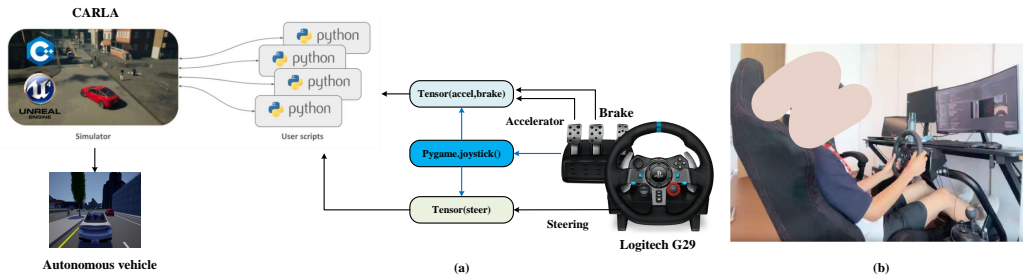


Figure 8: (a) CARLA connects with the G29 steering wheel (b) Human expert collects the datasets via the G29 steering wheel

A.5 Multiple types of input images

The 12 types of input data we designed are mainly categorized into single-modal and single-image input, single-image and multimodal fusion, and multiple images and multimodal fusion, as shown in Figure 9. We compare various input image types for evaluating the performance of NFRL, as shown in Table 2. ASD of lidar_noground reaches the highest value compared with all other input types. This is because lidar_noground removes a large amount of redundant information, reduces the difficulty of world model understanding environment semantics, and also involves stationary status of intelligent vehicle in experiment. The results show that the lidar_noground input is relatively optimal. However, it is worth noting that the effects of these 12 different input types are relatively small, with the ASD only varying between 20 and 40 meters. This shows that different data types have a minimal impact on the safety performance of intelligent vehicles.

1) **Single-modal and input of a single image.** As Figure 3 shown, the lidar images, which project the 3D point cloud information from lidar onto a 2D point cloud image, with each pixel color determined by whether there is lidar or other relevant pixel information on the corresponding area. Navigation

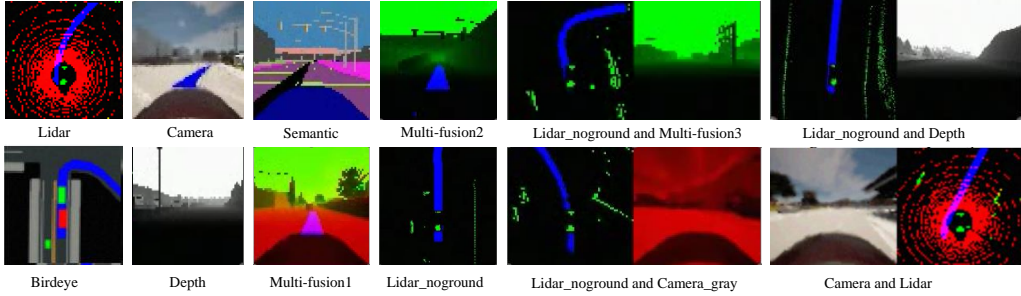


Figure 9: Multiple types of input images

Table 2: Evaluate the performance of NFRL under multiple input images in town03, training steps=100k. ASD is based on 5 episodes, the number of vehicles is 200.

Multiple input	ASD (m)
birdeye	29.4
lidar	38.6
camera	41.5
lidar + camera	56.4
semantic	26.3
depth	29.4
lidar_ng	64.7
multi-fusion1	52.1
multi-fusion2	47.2
lidar + depth_ng	32.5
lidar_ng + multi-fusion3	36.4
lidar_ng + camera_gray	48.8

path is rendered in blue and surrounding road conditions are represented by green rectangular boxes to indicate participants such as vehicles, pedestrians etc. Particularly, lidar_noground is created to remove redundant ground truth information from the 2D point cloud image. Moreover, we also consider camera, semantic, birdeye and depth as our sensor inputs.

2)**Single-image and multimodal fusion.** The input of single-image and multi-modal fusion involve fusing lidar, rgb forward-facing grayscale image(camera_gray), and navigation path into a composite rgb image with three types of information. The fused image has three channels, multi-fusion1(lidar,camera_gray,routing). Similarly having multi-fusion2(lidar,depth,routing) and multi-fusion3(lidar, depth,0).

3)**Multiple images and multi-modal fusion.** Multiple fusion can complement the shortcomings of a single input source and provide richer and more effective information. Therefore, we also design several single-modal fusion inputs as shown on the right side of Figure 3, including lidar_noground and multi_fusion3, lidar_noground and depth, lidar-noground and camera_gray, as well as camera and lidar.

A.6 Reward function

We use the following reward function f_2 in our experiments: where r_c is the reward related to collision, which is set to -1 if the ego vehicle collides and 0 otherwise. v_{lon} is the longitudinal speed of the ego vehicle. r_f is the reward related to running too fast, which is set to -1 if it exceeds the desired speed (8 m/s here) and 0 otherwise. r_o is set to -1 if the ego vehicle runs out of the lane, and 0 otherwise. α is the steering angle of the ego vehicle in radians. r_{lat} is the reward related to lateral acceleration, which is calculated by $r_{lat} = -|\alpha| \cdot v_{lon}^2$. The last constant term is added to prevent the ego vehicle from standing still. r_{ft} represents the time to collision in the forward direction, and if it is an autonomous vehicle and the time to collision with surrounding vehicles is below the safety threshold, this term is set to -1. r_{lt} represents the time to collision in the lateral direction, and if it

is an autonomous vehicle and the time to collision with surrounding vehicles is below the safety threshold, this term is set to -1. r_{sc} represents the smoothness constraint, and if the actual steering angle of the autonomous vehicle differs significantly from the predicted steering angle by the model, exceeding a set empirical constant, this term is set to -1.

$$\begin{aligned} f_1 &= 200r_c + v_{lon} + 10r_f + r_o - 5\alpha^2 + 0.2r_{lat} - 0.1 \\ f_2 &= f_1 + 200r_{ft} + 50r_{lt} + 2r_{sc} \end{aligned} \tag{15}$$

where the reward function f_1 is proposed by [9].

A.7 Hyperparameter settings

\mathcal{M}_{model} , the KL regularizer is clipped below 3.0 free nats for imagination range $H = 15$ using the same trajectories for updating action and value models separately with $\lambda = 0.99$ and $\lambda = 0.95$, while $k = 1.5$. The size of all our training and evaluating images is $128 \times 128 \times 3$. A random seed $S = 5$ is used to collect datasets for the *ego* vehicle before updating the model every $C = 100$ steps during training process.

A.8 The world model reconstructs the input images from the original sensors

We explore the differences between input images from original sensors and the corresponding reconstructed input images from a world model for 8 types of input. As shown in Figure 10, multiple comparisons are made between the reconstructed input types generated by the world model and their corresponding original sensor inputs. Among them, multi-fusion2, lidar_noground, lidar+camera and lidar reconstructions are very clear and highly consistent, indicating that $q(o_t|s_t)$ has a precise decoding capability without causing loss of s_t . However, birdeye, semantic, (lidar_noground and multi-fusion3), and (lidar_noground and camera_gray) of reconstructions are not as clear as their sensor input. This suggests that world model have difficulty understanding large amounts of irrelevant information related to driving tasks resulting in unclear reconstruction outputs.

Table 3: Hyperparameter settings for the training and evaluation of each baseline

Method	batch size	model size	eval episodes	action repeat
DDPG	256	32	5	2
SAC	256	32	5	2
TD3	256	32	5	2
DQN	256	32	5	2
Latent_SAC	256	32	5	2
Dreamer	256	32	5	2
NFRL	32	32	10	1
NFRL+SC	32	32	10	1
BC+Demo	32	32	10	1
NFRL+SC+Demo	32	32	10	1

Table 4: Hyperparameter settings for the learning rate of each baseline

Method	model learning rate	actor learning rate	value learning rate
DDPG	1×10^{-4}	3×10^{-4}	3×10^{-4}
SAC	1×10^{-4}	3×10^{-4}	3×10^{-4}
TD3	1×10^{-4}	3×10^{-4}	3×10^{-4}
DQN	1×10^{-4}	3×10^{-4}	3×10^{-4}
Latent_SAC	1×10^{-4}	3×10^{-4}	3×10^{-4}
Dreamer	1×10^{-3}	8×10^{-5}	8×10^{-5}
NFRL	1×10^{-3}	8×10^{-5}	8×10^{-5}
NFRL+SC	1×10^{-3}	8×10^{-5}	8×10^{-5}
BC+Demo	1×10^{-3}	8×10^{-5}	8×10^{-5}
NFRL+SC+Demo	1×10^{-3}	8×10^{-5}	8×10^{-5}

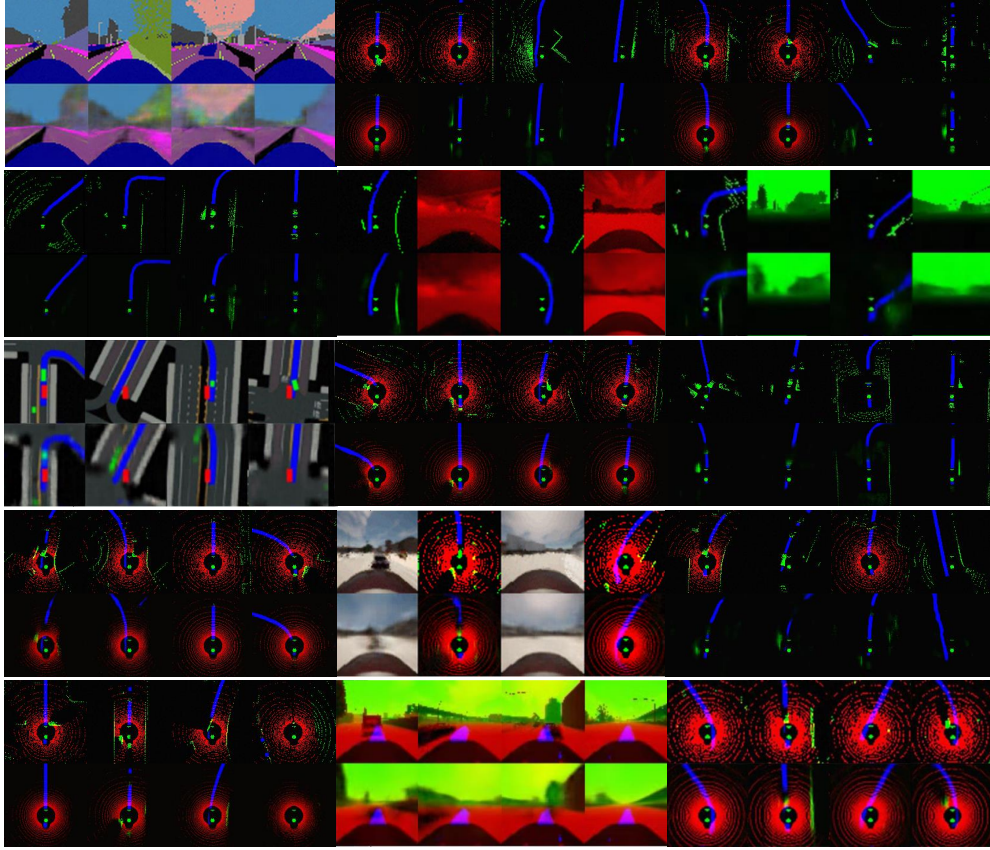
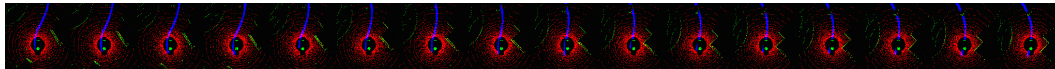
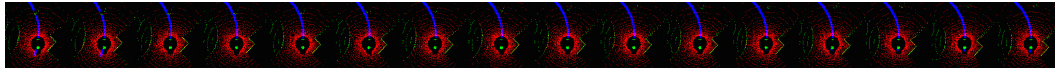


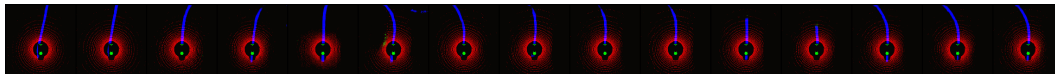
Figure 10: Randomly sampled frames to reconstruct the input images from the original sensors of EGADS on 8 types of input. For each type of image, first row: original sensor inputs. Second row: reconstructed images.



(a) Randomly sample ground truth of inputs Lidar o_1, o_2, \dots, o_{15}



(b) Randomly sample ground truth of inputs Lidar $o_{16}, o_{17}, \dots, o_{30}$



(c) Our model can imagine driving behaviors $\hat{o}_{16}, \hat{o}_{17}, \dots, \hat{o}_{30}$

Figure 11: We randomly sampled input images, and then EGADS was used to make predictions

A.9 More results regarding predictions of future driving trajectories

The accurate prediction of future driving trajectories is a precondition for making optimal decision making. Random samples of driving trajectories for the first 15 time steps were collected from the sensor. Subsequently, the model predicted the driving trajectories for the next 15 time steps, and the ground truths for these trajectories were also provided. We provide additional results regarding predictions of future driving trajectories as shown in Figure 11 ... Figure 14.

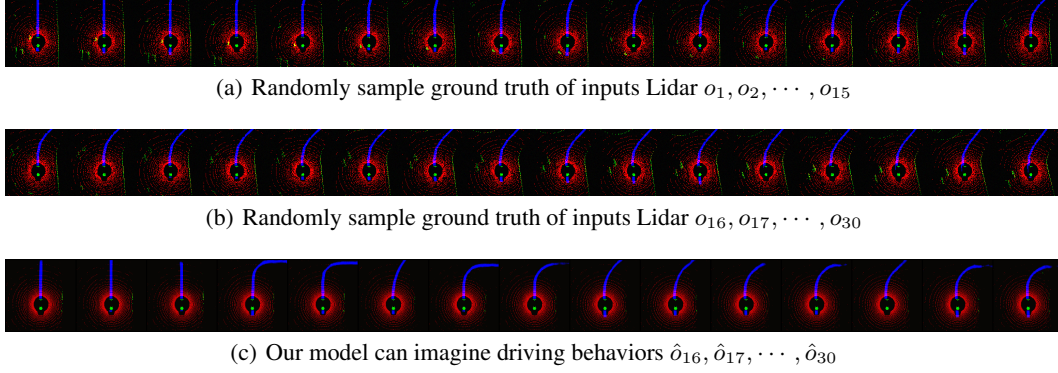


Figure 12: We randomly sampled input images, and then EGADS was used to make predictions

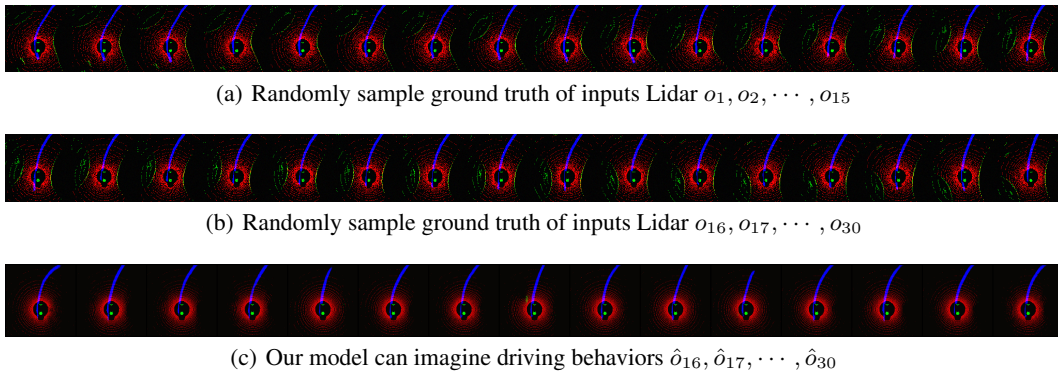


Figure 13: We randomly sampled input images, and then EGADS was used to make predictions

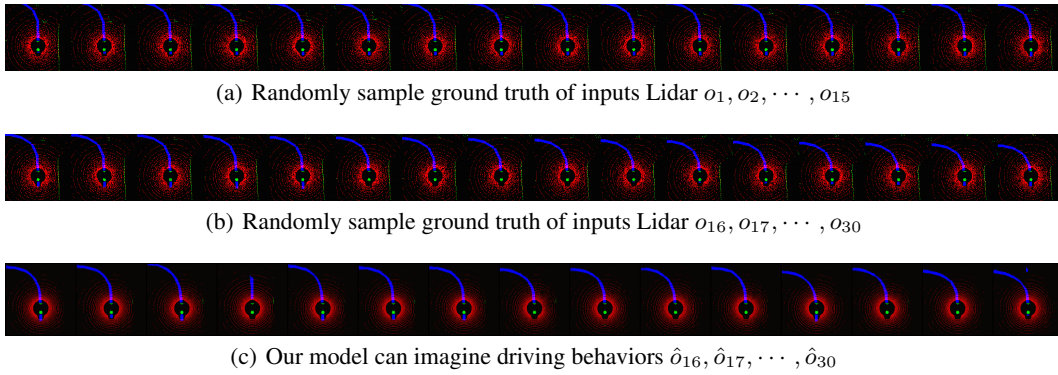


Figure 14: We randomly sampled input images, and then EGADS was used to make predictions